energies

MDPI

Article

Photoelectrochemical Hydrogen Production by Screen-Printed Copper Oxide Electrodes

Angela Gondolini *, Nicola Sangiorgi, Alex Sangiorgi and Alessandra Sanson

Institute of Science and Technology for Ceramics (ISTEC) of the National Research Council (CNR), Via Granarolo 64, 48018 Faenza, Italy; nicola.sangiorgi@istec.cnr.it (N.S.); alex.sangiorgi@istec.cnr.it (A.S.); alessandra.sanson@istec.cnr.it (A.S.)

* Correspondence: angela.gondolini@istec.cnr.it; Tel.: +39-0546-699-743

Abstract: In this work, copper oxides-based photocathodes for photoelectrochemical cells (PEC) were produced for the first time by screen printing. A total 7×10^{-3} g/m^2 glycerine trioleate was found as optimum deflocculant amount to assure stable and homogeneous inks, based on CuO nano-powder. The inks were formulated considering different binder amounts and deposited producing films with homogenous thickness, microstructure, and roughness. The as-produced films were thermally treated to obtain Cu_2O- and Cu_2O/CuO-based electrodes. The increased porosity obtained by adding higher amounts of binder in the ink positively affected the electron transfer from the surface of the electrode to the electrolyte, thus increasing the corresponding photocurrent values. Moreover, the Cu_2O/CuO system showed a higher charge carrier and photocurrent density than the Cu_2O-based one. The mixed Cu_2O/CuO films allowed the most significant hydrogen production, especially in slightly acid reaction conditions.

Keywords: water splitting; hydrogen; screen-printing; CuO-based electrode

Citation: Gondolini, A.; Sangiorgi, N.; Sangiorgi, A.; Sanson, A. Photoelectrochemical Hydrogen Production by Screen-Printed Copper Oxide Electrodes. *Energies* **2021**, *14*, 2942. https://doi.org/10.3390/en14102942

Academic Editor: Dmitri A. Bulushev

Received: 25 February 2021
Accepted: 12 May 2021
Published: 19 May 2021

1. Introduction

The increasing global warming and the need to adopt alternative energy sources push researchers to find clean and sustainable solutions for energy generation, conversion, and storage. Hydrogen represents a clean energy vector that can be used to store the excess energy coming from renewable sources, reducing their intrinsic intermittency. In this context, photoelectrochemical cell (PEC) water splitting is one of the most promising technologies for producing hydrogen with a low environmental impact [1–3]. Several efforts have been recently focused on the production of high-performing and durable electrodes [2,4,5]. Nevertheless, the major challenge in this area remains the development of reliable, robust, cost-effective, efficient, and stable semiconducting electrodes. Copper oxides are promising photocathode materials for this application, thanks to their high optical absorption, suitable bandgap for water reduction, p-type properties, low cost, and high abundance [2,6]. Cu_2O in particular, due to its optical gap (2.62 eV) and direct bandgap energy (1.9–2.17 eV) [2,7–9] is mostly considered for the water reduction under visible light. CuO produced by thermal treatment on Cu_2O moreover, can improve the photoelectrode response and act as a protective layer against Cu_2O photocorrosion [10]. The activity of copper-based materials used for PEC applications, however, strongly depends on the deposition methods used for their fabrication [11]. Furthermore, the recent interest in the development of PEC systems beyond laboratory scale have shifted the attention to those shaping methods able to realize large-area electrodes. There are numerous methods that have been proposed to produce lab-scale copper-based electrodes for water splitting: sol-gel spin coating [8], electrodeposition [7,12], flame-spray pyrolysis [13], sputtering [14], etc. Among the others, dip-coating, spin-coating, and electrodeposition techniques are considered simple and cost-effective shaping methods. However, dip- and spin-coating show some limitations linked to the film quality control and efficiency for large-scale

production [15]. On the other hand, electrodeposition has been largely employed for film production for PEC application as a versatile, low-cost, and easy-scalable technique. The main drawbacks related to this method are linked to the impurities of the deposited layer due to the presence of other ionic species [16] and to the large volume of electrolyte consumed, in particular for large-scale processes. In this paper we consider, therefore, screen printing for electrodes deposition, due to its numerous advantages in terms of reproducibility, cost effectiveness, and potential for large-scale fabrication [4,17,18]. With this method, an ink containing the photocatalyst is prepared and deposited through a screen onto a suitable substrate. After drying and sintering, the resulting film is stable and well-adherent to the chosen substrate. Other advantages of this technique are the homogeneity of the resulting film, even for large areas; and the possibility of easily modulating the chemical composition of the ink [19]. For the production of PEC electrodes, the ink is generally deposited on transparent conducting substrates like fluorine-doped tin oxide glass (FTO), which allows the optical radiation transmission needed to activate the photoelectrochemical processes, and the electrical conductivity. One of the main issues in PEC is the instability of many semiconducting materials in extremely acidic or alkaline electrolyte solutions [20]. For this and for safety reasons, many researchers start to study reactions in electrolytes with near-neutral pH; enabling, in this way, also the use of seawater [20]. In this work, screen-printing inks of CuO were formulated and prepared, with the composition optimized in terms of its deflocculant nature and amount of binder. The influence of the inks' chemical compositions on the electrochemical/photoelectrochemical properties of screen-printed Cu-based electrodes were studied and considered for water-splitting applications. Two inks were then selected for the development of approximately 2–2.5 µm thick electrodes. The as-produced films were fully characterized from the optical and photoelectrochemical points of view in order to correlate the ink compositions and film morphologies to their functional properties. The hydrogen production of the obtained films was finally evaluated by a three-electrode photoelectrochemical cell under illumination at slightly acid reaction conditions. The development of a suitable ink is fundamental for the screen-printing process and consequently for the upscaling of these devices. To the authors' best knowledge, there are no other works on screen-printed copper oxide-based electrodes for photoelectrochemical cell (PEC) water-splitting applications.

2. Materials and Methods

2.1. Electrodes Development

Commercially available CuO (Sigma Aldrich, Milano, Italy) with specific surface area (SSA) of 5.81 m^2/g, was used as a starting material for inks production. Terpineol (Sigma Aldrich) was considered as solvent, and ethyl cellulose (EC, Sigma Aldrich) as binder. The powder content was fixed at 10 vol% in respect to the solvent volume, and the most appropriate deflocculant was added directly to the powder suspension. The as-prepared inks were milled in a three-roll mill (Exakt 80E, Norderstedt, Germany). Finally, the prepared inks were deposited with a semi-automatic screen printer (AUR'EL 900, AUREL Automation S.p.A., Modigliana, Italy) on the surface of conductive glass slides (FTO, Sigma Aldrich 7 Ω/sq). The final size of the electrodes was 13 × 18 mm^2. The layers were then dried in an IR furnace (Ero Electronic SrL, Novara, Italy) at 80 °C for 15 min and thermally consolidated in air (Hobby 35, Nabertherm, Lilienthal, Germany) or in 4% H_2/Ar atmosphere (RHTH 120-600/16, Nabertherm, Lilienthal, Germany).

2.2. Inks and Electrodes Characterization

Glycerin trioleate (GTO, Sigma Aldrich), Span 80 (Fluka, Milano, Italy), Tween 20 (Sigma Aldrich), lauric acid (LA, Sigma Aldrich), and furoic acid (FA, Sigma Aldrich) were considered as possible deflocculants. The best type of deflocculant was chosen through viscosity measurements. The suspensions for these tests were prepared with the powder content reported above, and ball-milled for 15 min after the deflocculant addition. Viscosity measurements of the solvent-powder-deflocculant suspension and of

the inks were performed using a controlled-stress rheometer (Bohlin CVOR 120, Malvern Instruments, Rome, Italy, plates diameter = 25 mm), setting the gap between the plates at 500 µm. These measurements were done at the minimum and maximum values of shear rates from 0.02 to 70 s^{-1}, respectively. The thermogravimetric and differential scanning calorimetry (TG-DSC) tests of the inks were carried out in a thermal analyzer (STA 449, Netzsch, Selb/Bavaria, Verona, Italy) at 10 °C min^{-1} as heating rate. The electrode microstructures were investigated by FE-SEM (field emission gun-scanning electron microscopy SIGMA, Zeiss, Oberkochen, Germany). The average porosity of the produced electrodes was digitally determined (Image J). The thickness and the average surface roughness parameters (Ra) of the films were measured using an optical microscope (Contour GT-K 3D, Bruker, Berlin, Germany) equipped with a 5× lens and applying the ISO 4287 standard and a Gaussian filter. The bandgap energy (E_g) was calculated from the diffuse reflectance analysis using an integrating sphere and PVE300 system (BENTHAM Instruments Ltd., Reading, UK) calibrated with $BaSO_4$ as reference. All reflectance spectra were converted following the Kubelka–Munk function (KM) [21] and the obtained values were used in the Tauc equation:

$$\alpha h\upsilon = A\left(h\upsilon - E_g\right)^n \quad (1)$$

where α is absorption coefficient (proportional to KM function), h is the Planck's constant (J·s), light frequency (s^{-1}) is ν, the absorption constant is A, and E_g is the bandgap energy. n refers to the electronic transition, which can be an indirect allowed transition equal to 2, indirect forbidden transition equal to 3, 1/2 for the direct allowed ones, and 3/2 for direct forbidden transitions [21]. In this work n was considered equal to 1/2 [22,23]. All the electrochemical and photoelectrochemical measurements were carried out using an electrochemical working station (Autolab-PGSTAT302N + FRA32M Metrohm, the Netherlands) in a three-electrode cell with a platinum wire as a counter electrode, Ag/AgCl (KCl 3.5 M) as a reference electrode, and FTO with a screen-printed copper layer as a working electrode. The active area analyzed was set at 0.5 cm^2, while as electrolyte a solution of 0.1 M Na_2SO_4 (Sigma Aldrich) in water MQ (pH 5.8) was considered. Before the measurement, the solution was purged with argon for 15 min to remove oxygen. Mott–Schottky (MS) analyses were done in the potential range between +0.8 V and −0.8 V vs. SCE (starting from the anodic potential) and in a frequency range between 10 KHz to 0.5 Hz with 10 mV amplitude of the AC signal. The Mott–Schottky plots were obtained at 1 KHz, and the flat-band potential (E_{fb}) and the number of majority charges (N_A) were identified using the Mott–Schottky equation:

$$\frac{1}{C^2} = \frac{2}{\varepsilon\,\varepsilon_0 e N_A}\left(E - E_{fb} - \frac{k_B T}{e}\right) \quad (2)$$

where C is the specific capacitance (F) extrapolated from the EIS analyses, ε is the dielectric constant of the semiconductor (7.6 and 10.26 for Cu_2O and CuO respectively) [23], ε_0 is the dielectric vacuum permittivity (8.85, 419 × 10^{-12} C^2 J^{-1} m^{-1}), e is the elementary charge (1.602176 × 10^{-19} C), E is the applied potential (V), k_B is the Boltzman constant (1.38065 × 10^{-23} J K^{-1}), and T is the temperature (298 K). Finally, the photocurrents were determined by linear scan voltammetry (LSV) under stirring and light/dark conditions. The intensity of 1000 W m^{-2} was calibrated with a reference certified silicon cell (Lot–Oriel). The potential was swept between 0 and −1.0 V vs. Ag/AgCl at a scan rate of 20 mV/s.

2.3. Hydrogen Production

All the deposited films were used as photoelectrodes for the hydrogen production via water splitting. The three-electrode photoelectrochemical cell previously described was used for this purpose and chronoamperometry were conducted at a constant potential of −1.5 V vs. Ag/AgCl for 2 h. The gas samples were analyzed every 10 min using a 990 micro-GC (Agient Technologies) equipped with a Molecular sieve 5Å packed column

for hydrogen detection and a thermal conductivity detector (TCD); argon was used as carrier gas.

3. Results and Discussion

The SEM micrograph of the CuO starting powder used for the ink development (Figure 1) shows the presence of micrometric spheric aggregates of nanometric particles.

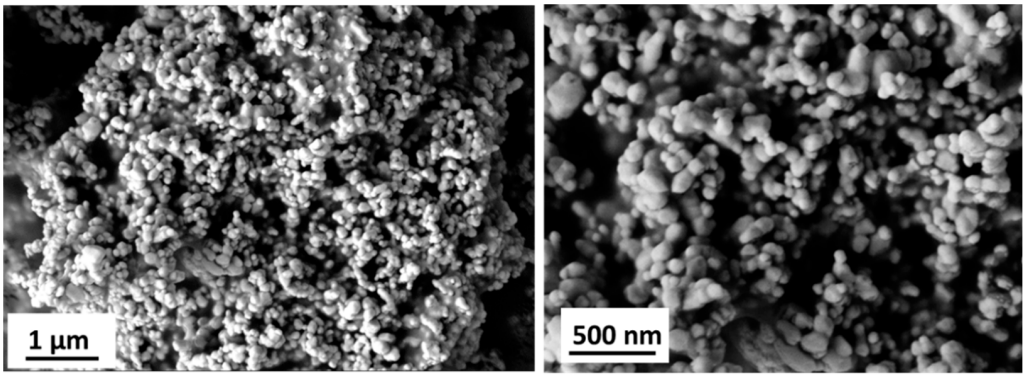

Figure 1. SEM micrographs of the CuO powder considered in this study.

The ink compositions were studied starting from the amount and nature of deflocculant needed to produce stable terpineol-based slurries. The ink stability is in fact, strongly linked to the stability of the powder suspension. On the other hand, the stability of the suspension depends on the effectiveness of the coordination sphere around the particles [24] that can be improved using a deflocculant. The latter acts on the particles through one or two mechanisms eventually combined: electrostatic repulsion or steric stabilization [25,26]. Among the dispersants chosen, glycerol trioleate (GTO) and Span 80 have a prevailing steric effect; furoic acid (FA) shows mainly an electrostatic behavior; while lauric acid (LA) and Tween 20 show a combination of electrostatic and steric activity. Rheological tests on suspensions with the same powder concentration of the inks were selected in order to find the most effective dispersant for the CuO system [25,26]. Different dispersant amounts (g dispersant for m^2 of powder) were tested in the range between 3×10^{-4} to 9×10^{-3} [27]. The values of the suspension viscosities were determined at a shear rate of 1 s^{-1}, the value of shear to which an ink is typically subjected at the beginning of the printing process. The results, reported in Figure 2, show that the deflocculants that mainly or partially have an electrostatic action (LA, FA, and Tween 20) were not effective in stabilizing the system. On the other hand, the viscosity of the suspensions decreases when deflocculants with steric behaviour (GTO and Span 80) were added. Among the different concentrations tested for these two systems, 7×10^{-3} g/m^2 GTO gave the best stabilization and was therefore considered as deflocculant for the CuO inks.

The binder plays a fundamental role in determining the printability of a screen-printing ink [28]. For this reason, different concentrations of binder were tested. CuO inks were then produced considering 25, 35, 45, and 55 vol.% of binder in respect to the powder. The compositions of the different inks are reported in Table 1.

Table 1. Compositions of the CuO inks (vol.%).

Material	Ink_25	Ink_35	Ink_45	Ink_55
CuO	8.54	8.39	8.20	7.94
Terpineol	85.40	83.92	81.99	79.37
GTO	3.21	3.16	3.08	2.98
EC	2.85	4.53	6.72	9.71

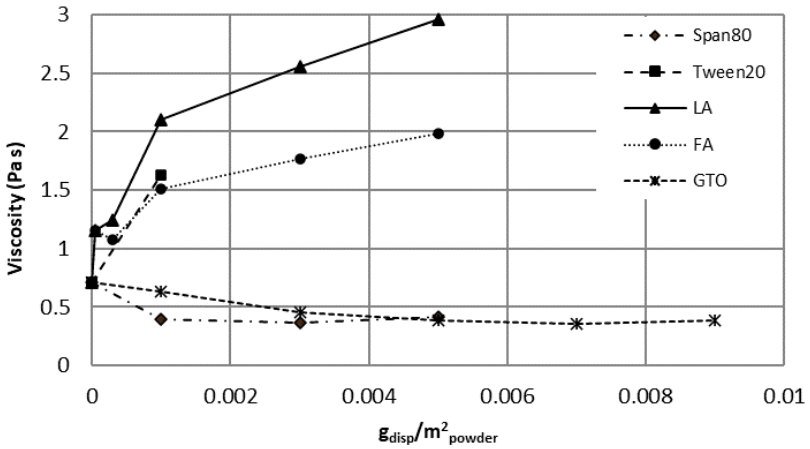

Figure 2. Viscosity of the CuO-terpineol suspensions produced using different types and concentrations of deflocculants.

The flow curves of the four inks are presented in Figure 3. These data show a typical pseudoplastic behaviour for all the formulations with viscosity suitable for the screen-printing process [17]. Particularly, the polymeric network is more structured for higher binder contents, as shown by the increase in inks viscosity passing from ink_25 to ink_55.

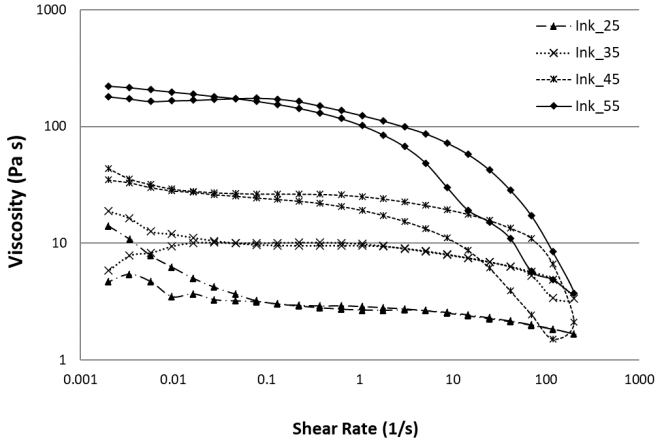

Figure 3. Flow curves of the formulated CuO inks.

The TG–DSC analysis of one of the inks produced is reported, as example, in Figure 4. This analysis shows two main weight losses at about 150 and 300 °C, due to the solvent evaporation and organics removal, respectively. The analyses of inks with different compositions, differing just on the amount of employed organics and therefore on the weight loss on the TG curve, are not here presented.

The layers produced after drying were treated at 450 °C for 10 min in reducing atmosphere in order to eliminate all the organics and obtain a well-consolidated electrode structure. The SEM images of the produced layers reported in Figure 5 shows homogeneous and crack-free films.

The film roughness was investigated by non-contact profilometry (Table 2).

Table 2. Roughness data of the CuO-based films.

Parameter	Ink_25	Ink_35	Ink_45	Ink_55
Ra (μm)	0.515 ± 0.063	0.412 ± 0.059	0.415 ± 0.085	0.372 ± 0.076

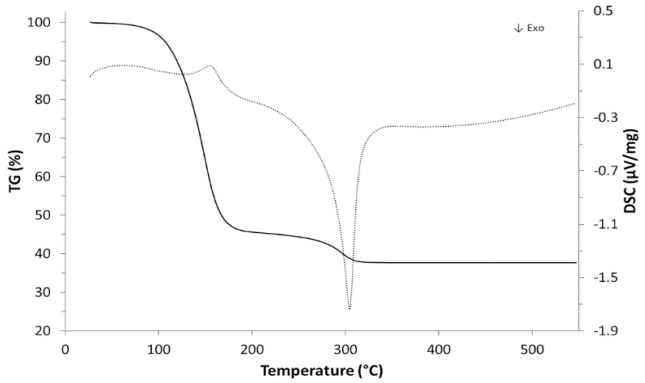

Figure 4. TG–DSC analysis of one of the inks produced.

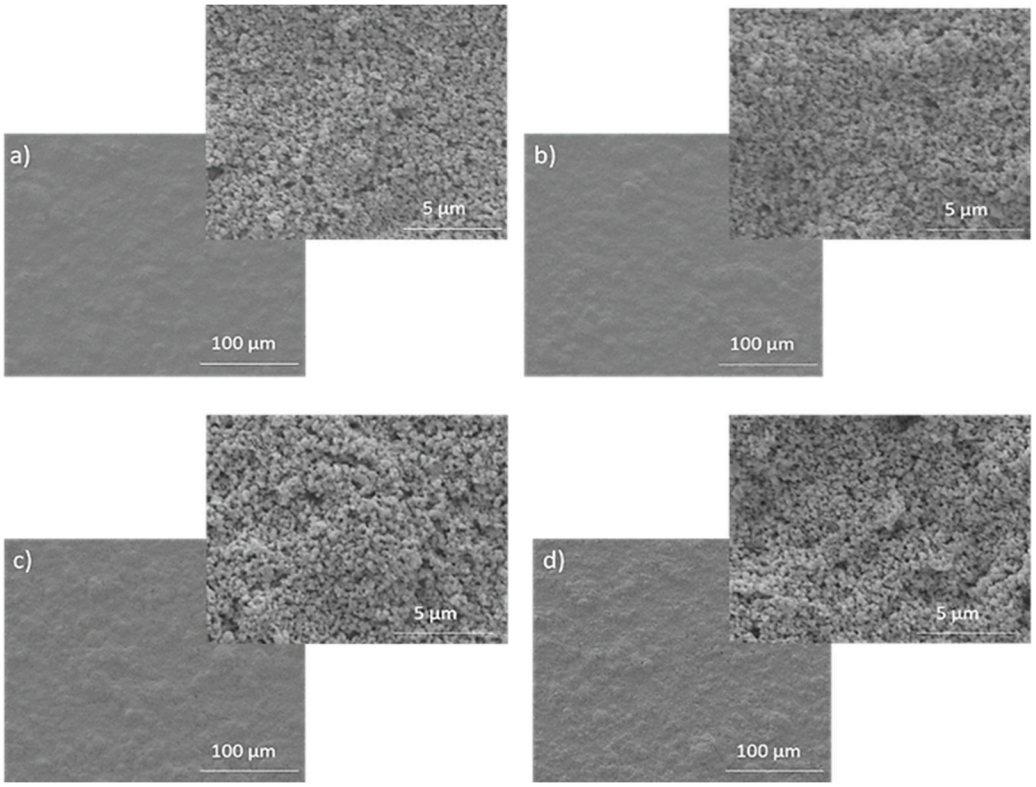

Figure 5. SEM images of the surfaces of the electrodes produced using (**a**) ink_25, (**b**) ink_35, (**c**) ink_45, and (**d**) ink_55.

The reported Ra values indicate that a higher binder amount leads to smoother surfaces going from 0.515 ± 0.063 µm down to 0.372 ± 0.076 µm for ink_25 and ink_55 respectively. The corresponding 3D projections (area 1 mm^2) are reported in Figure 6.

Figure 6a, corresponding to ink_25, shows a surface densely covered by sharp particle agglomerates, while an increase in the binder amount (Figure 6b), generates a less defective area. Since the performances can change significantly with the electrodes' microstructures [18,29], the samples produced with compositions containing the higher and the lower amount of binder (ink_25 and ink_55), were selected for the functional analyses. These electrodes showed the higher difference in porosity (48 ± 3 vol.% for ink_25 and 56 ± 2 vol.% for ink_55) and surface roughness (Table 2). To compare the results obtained, the layers were produced with similar final thicknesses: 2.10 ± 0.73 and 2.29 ± 0.66 µm for ink_25 and ink_55, respectively. After the thermal treatment in reducing atmosphere, the XRD results of Figure 7 show the presence of Cu_2O (JCPDS 05-0667) and Cu (JCPDS 3-065-9026) in the electrodic layer. In literature it is reported [30] that the reduction of Cu

follows the path: CuO→Cu_2O→Cu. The presence of different species is therefore related to strength of the reduction process. To increase the amount of Cu(I), one of the most promising photocatalysts for the conversion with visible light [9], the layers produced were oxidized using further thermal treatments in air (with dwelling time of 30 min). The annealed electrodes showed changes in film composition, as reported in the XRD spectra of Figure 7. The nature of the phases present changed with temperature, increasing the percentage of the oxidized copper forms, following this oxidation path Cu→Cu_2O→CuO. Cu_2O (JCPDS 05-0667) is present at 250 °C, at 350 °C CuO (JCPDS 48-1548) is the only phase present, while the treatment at 300 °C (medium temperature) shows the coexistence of Cu_2O/CuO. The films treated at 250 (Cu_2O) and 300 °C (Cu_2O/CuO) were then selected for the functional characterizations. It is worth remembering that a mixture of Cu_2O and CuO could assure good photocatalytic properties as well as sufficient stability against photocorrosion.

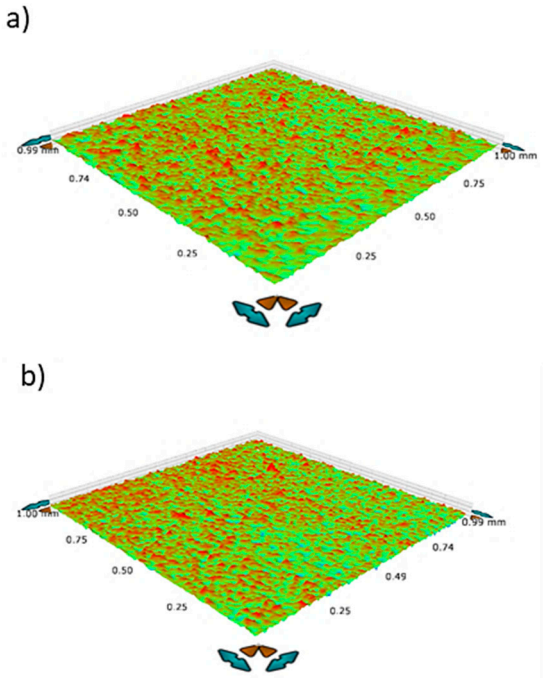

Figure 6. Optical profilometer 3D images of the films obtained using (**a**) ink_25 and (**b**) ink_55.

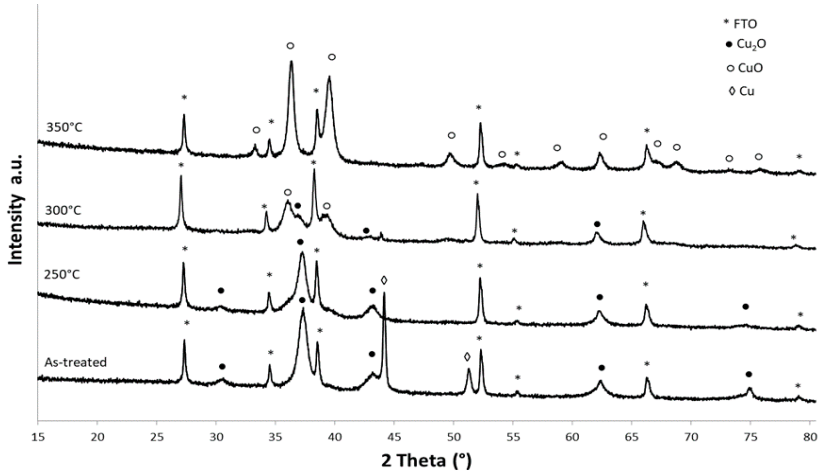

Figure 7. XRD patterns of the as-sintered electrode (as-treated) after oxidation treatment at 250 and 350 °C for 30 min.

The bandgap energy (E_g) is one of the most important optical properties required for a photoelectrode to drive a sunlight reaction. Figure 8a,b shows the UV–Vis diffuse reflectance spectra of the films based on ink_25 and ink_55 treated at different temperatures (250 and 300 °C). The samples treated at 250 °C (Cu_2O) show an adsorption edge at ca. 550 nm while the ones oxidized at 300 °C (Cu_2O/CuO) extend their absorption edge at ca. 900 nm due to the low bandgap value of CuO [22,23]. The E_g values for each sample were determined from reflectance spectra using the Kubelka–Munk function and Equation (1). The obtained Tauc plots and the extrapolated values are reported in Figure 8c, d and Table 3.

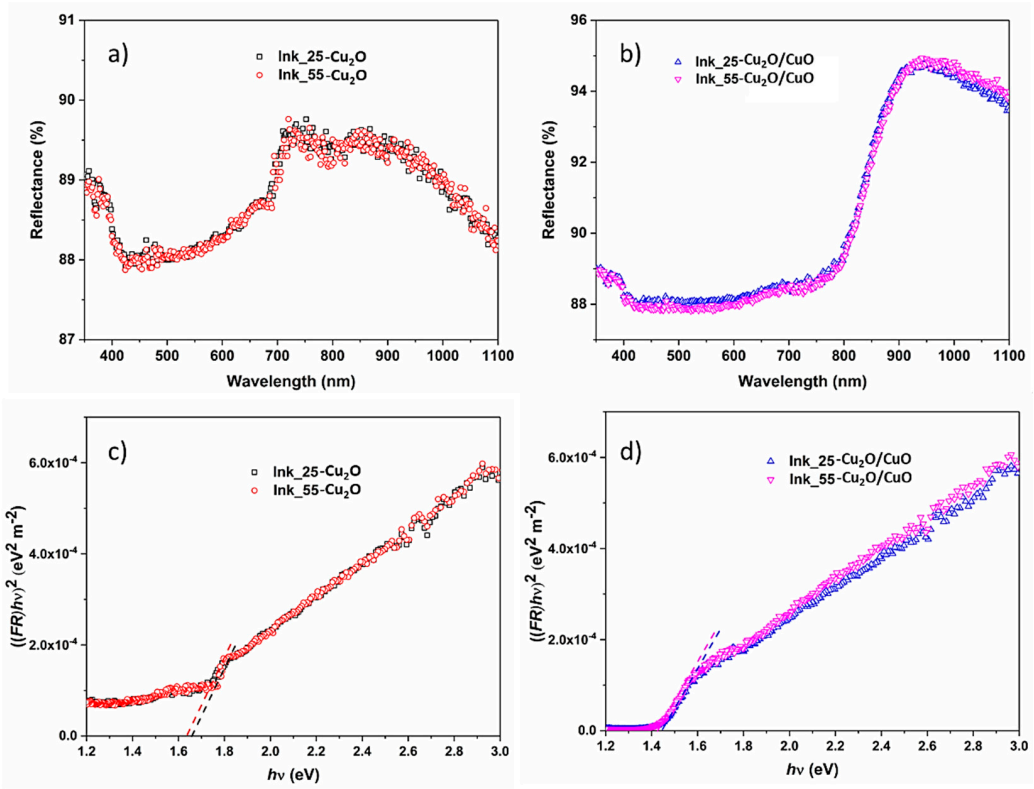

Figure 8. UV–Vis diffuse reflectance spectra of films produced with Cu_2O-based ink (**a**) and Cu_2O/CuO-based ink (**b**), and related Tauc plots for Cu_2O-based ink (**c**) and Cu_2O/CuO-based ink (**d**).

Table 3. Bandgap values calculated from Figure 8, flat-band potential (E_{fb}) and number of donors (N_A) for the prepared photoelectrodes.

Phase	Inks	E_g (eV)	E_{fb} (V) vs. Ag/AgCl	E_{fb} (V) [a] vs. NHE	N_A (cm^{-3})
Cu_2O-based	Ink_25	1.65	0.58	1.12	2.6×10^{27}
	Ink_55	1.63	0.62	1.16	2.3×10^{27}
Cu_2O/CuO-based	Ink_25	1.46	0.61	1.15	2.5×10^{28}
	Ink_55	1.44	0.66	1.20	2.4×10^{28}

[a] calculated using the equation E (V) vs. NHE = E (V) vs. Ag/AgCl (V) + 0.059pH + 0.197 V [31].

Table 3 shows comparable bandgap values for Cu_2O and Cu_2O/CuO-based films, respectively. The obtained results are in good agreement with the ones reported in literature [23,32]. For the Cu_2O/CuO-based layers, the bandgap values decrease compared with the layers of Cu_2O, due to the combination of the different copper phases produced by the different thermal treatments that finally extends the light adsorption range. The ability of Cu_2O/CuO to harvest photons with higher energy can improve the hydrogen production

when this electrode is used as a photocathode in PEC, as reported by P. Diao et al. [23]. The electronic properties of the screen-printed films were determined using equation 2. The obtained Mott–Schottky plots are reported in Figure 9 and the flat-band potential (E_{fb}) and number of donors (N_A) are reported in Table 3.

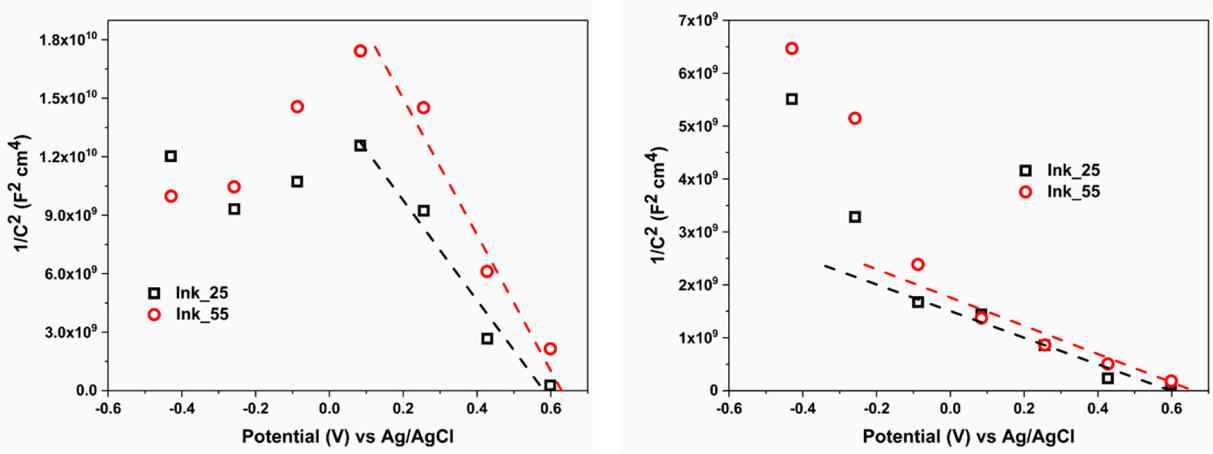

(**a**) (**b**)

Figure 9. Mott–Schottky plots of Cu_2O-based (**a**) and Cu_2O/CuO-based (**b**) films.

A negative slope was obtained for each Mott–Schottky plot indicating that these materials are p-type semiconductors and thus suitable as cathodes for the water-splitting reaction. This is due to their ability to use the photogenerated electrons to drive the reduction of water to hydrogen. From the Mott–Schottky equation and considering the slope of the linear part of the curves reported in Figure 9 and the intercept on the *x* axes (at $1/C^2$ equal to 0), the majority carrier density (N_A) and flat-band potential (E_{fb}) were estimated. The corresponding values are reported in Table 3 where the flat-band potential is also converted into reference potential scale NHE. The highest N_A was obtained for the Cu_2O/CuO films, indicating a fast charge transfer from the photoelectrode surface to the electrolyte, and slow charge recombination mechanisms [23,31]. Moreover, higher flat-band potential values were obtained for the films based on Cu_2O/CuO, indicating (for a p-type semiconductor) a higher degree of band bending; this induces a large driving force to separate the photoinduced charges in the space charge region [31,32]. Both higher number of donors and flat-band potential contribute to enhance the photocurrent and PEC performances. For p-type semiconductor, the E_{fb} values could be taken as a reasonable approximation ($\leq$100 mV) to the valence band position (VB), while the conduction band position (CB) can be evaluated adding to the VB the E_g value previously calculated (Table 3). The obtained CB positions are equal to −0.53 V and −0.47 V vs. NHE for Cu_2O-based films on ink_25 and ink_55 respectively, and −0.31 V and −0.24 V vs. NHE for Cu_2O/CuO-based films on ink_25 and ink_55 respectively. These CB edges are more negative than the redox potential of the H_2O/H_2 reaction at the same pH environment for all the films tested, indicating that the photoinduced electrons in the conduction band can be efficiently injected into the electrolyte for the reduction of water. Linear scan voltammetry (LSV) in light/dark conditions was used to quantify the photocurrent produced by each film (Figure 10). High electrical conductivity was observed for each electrode in the wide potential range tested up to −1.0 V vs. Ag/AgCl. Considering the photoelectrodes based on Cu_2O, the photocurrents acquired are 0.026 mA cm^{-2}, 0.058 mA cm^{-2} for ink_25 and ink_55 respectively. The films based on a mixed Cu_2O/CuO were able to produce 0.040 mA cm^{-2} and 0.089 mA cm^{-2} (ink_25 and ink_55, respectively). The highest photocurrent densities were obtained (considering the same ink composition) for the films based on Cu_2O/CuO, due to the highest quantity of carriers available and the low amount of recombination phenomena that occurs at the photoelectrode surface. However, the higher porosity of the ink_55 films

(in respect to the Ink_25 ones) enhances the electron transfer from the electrode surface to the electrolyte increasing the photocurrent values.

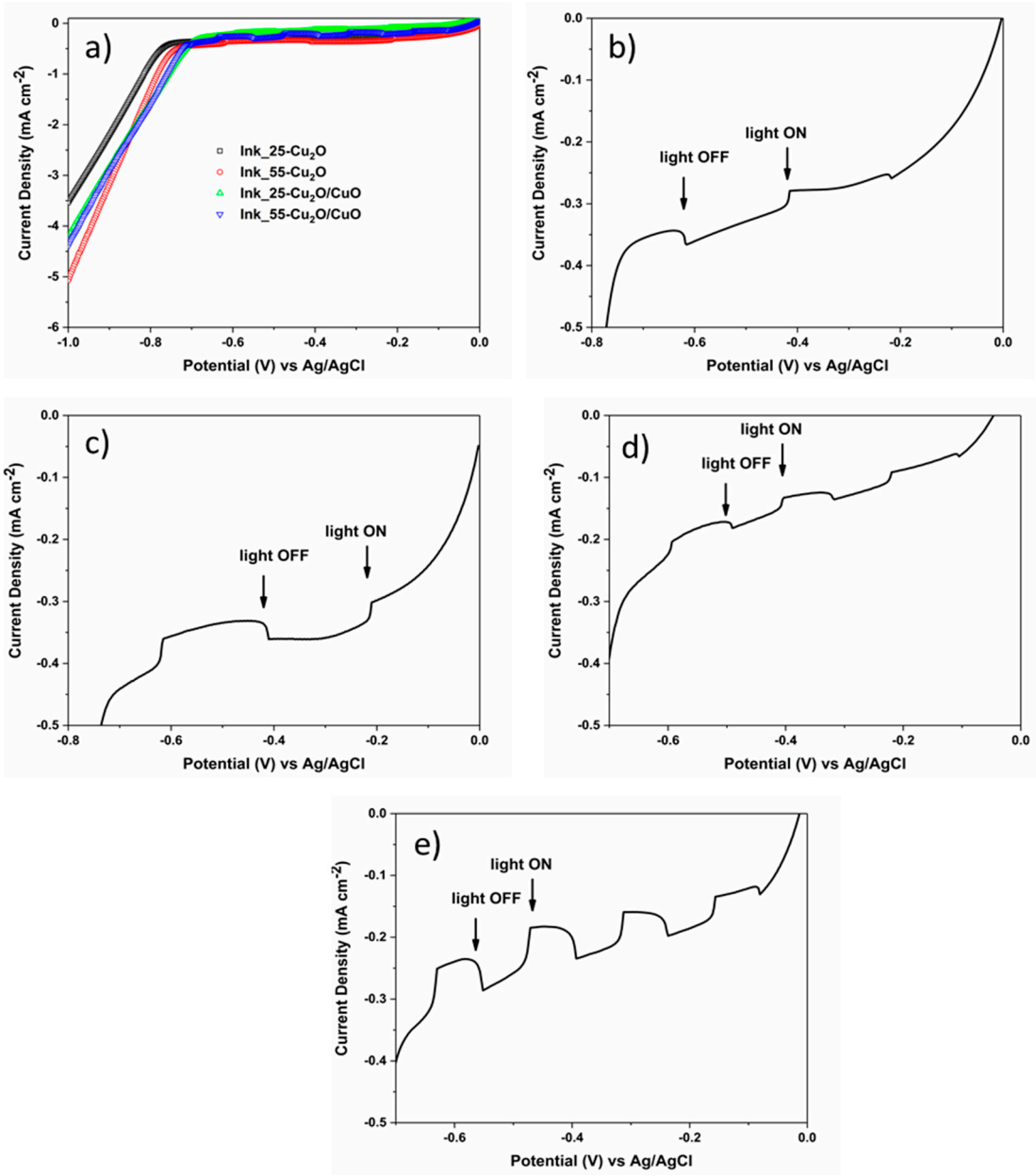

Figure 10. (**a**) Linear sweep voltammetry in light/dark conditions in a wide potential range, (**b**) magnification in the low potential range for films based on ink_25–Cu_2O, (**c**) ink_55–Cu_2O, (**d**) ink_25–Cu_2O/CuO, and (**e**) ink_55–Cu_2O/CuO.

The photoelectrodes thickness (2.10 ± 0.73 for ink_25 and 2.29 ± 0.66 µm for ink_55) deeply influenced the photocurrent produced. Films with thicknesses close to 1 µm reported in literature [23] achieved, at pH = 6 and 0 V vs. NHE, photocurrents of 0.25 mA cm^{-2} (Cu_2O) and 2.5 mA cm^{-2} (Cu_2O/CuO). On the other hand, Teng et al. [33] reports for a 16-µm-thick Cu_2O photoelectrode prepared by electrochemical deposition 0.024 mA cm^{-2} at −0.5 V vs. Ag/AgCl at pH = 6. The higher film thicknesses used in this work induced a decrease of the photocurrent values, due to the highest diffusion length of the photogenerated majority charges [34]. Moreover, in the absence of a protective layer, a high degree of photocorrosion phenomena negatively influences the photocurrent values achieved [35,36].

The hydrogen production tests were done using Cu_2O and Cu_2O/CuO films as photoelectrodes. The reaction time was set at 2 h with a constant applied potential of −1.5 V vs. Ag/AgCl; the amount of hydrogen produced is reported in Figure 11. When light reaches the photoelectrode, copper oxide can absorb photons (due to its bandgap energy) and charge separation takes place at the interface of the valence and conduction bands. The photogenerated electrons are produced in the conduction band (CB) and the holes in the valence band (VB). Due to its p-type conductivity, electrons travel to the electrode surface/electrolyte interface where water reaction occurs by protons (H^+) reduction. To complete the redox cycle, photogenerated holes are transferred by the electrical connection to the counter-electrode where water oxidation take place. The highest value of hydrogen production was obtained for the Cu_2O/CuO system due to the contribution of the highest photocurrent previously observed, which increased the reaction rate. For both systems, the highest porosity of the film produced by adding more binder (ink_55) increases the amount of hydrogen produced, due to an augmented number of catalytic sites. However, in the case of Cu_2O/CuO-based electrodes, the hydrogen production is quite similar. This indicates that the influence of the microstructures on the electrode properties is lower than the nature of the present phase. These results are comparable with the one reported by H. Teng et al. [33] where a thicker Cu_2O film produced 4 µmol of hydrogen after 120 min in 0.5 M Na_2SO_4 electrolyte under irradiation.

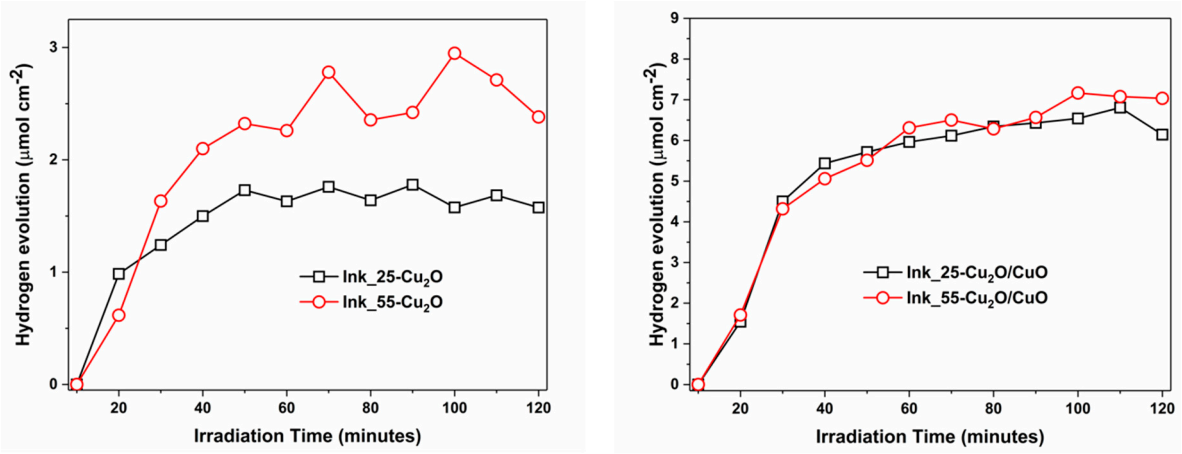

(**a**) (**b**)

Figure 11. Hydrogen evolution by photoelectrochemical cells with a working electrode based on (**a**) Cu_2O- and (**b**) Cu_2O/CuO-based films.

Figure 11 shows that hydrogen production increased linearly with reaction time up to 40 min for both the tested photoelectrodes. Different reaction rates were observed for CuO and Cu_2O/CuO samples and this behavior could be linked to in situ catalyst activation, due to the reduction to metal copper that finally enhances the electronic acceptor capacity [37,38].

The moderate amount of hydrogen produced is linked to the slightly acid conditions used (pH = 5.8). At low pH, the proton reduction to hydrogen dominates [37], therefore the H_2 development reaction is positively affected. Salts addition to acidify pH and increase ionic conductivity should, however, be avoided for a safe and sustainable large-scale hydrogen production PEC technology [20].

The post-operation analyses of the samples annealed at the two different temperatures (named Cu_2O and Cu_2O/CuO) were carried out to understand the effect of testing on the two-layer compositions. The XRD spectra of the post-operation electrodes are reported in Figure 12 and reveal the presence of metallic copper in both the compositions. These indicates the reduction of Cu-based species already reported by different authors for pure copper-oxide electrodes [10,39] leading to a progressive degradation of the films.

This can be also observed by the SEM micrographs of Figure 13 that show cracks on the films surfaces after operation. Further activities are ongoing to improve the copper-based electrode's life span in operation.

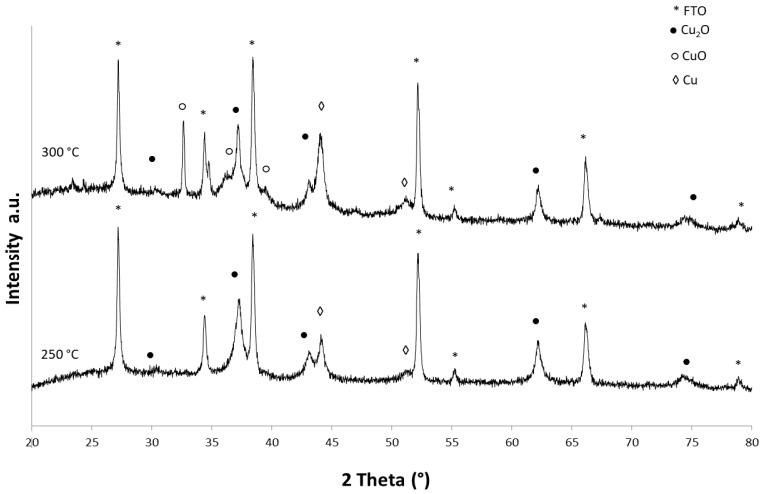

Figure 12. XRD patterns of the Cu_2O and Cu_2O/CuO electrodes after PEC test.

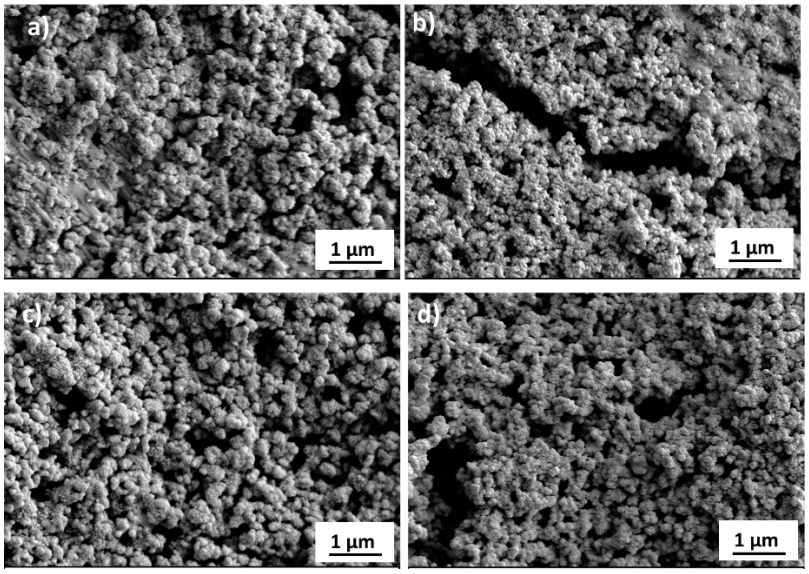

Figure 13. SEM images of ink_250 (**a**) and ink_300 (**c**) before the PEC test; and ink 250 (**b**) and ink_300 (**d**) after PEC measurements.

4. Conclusions

In this work, CuO screen-printing inks were successfully formulated and deposited on FTO glasses to produce photocathodes for the water-splitting process. Glycerine trioleate was selected as the best deflocculant, in the amount of 7×10^{-3} g/m^2, to produce stable and homogeneous inks. These were formulated using different binder amounts and deposited, producing films with homogenous thickness and microstructure, and suitable values of roughness. Inks containing 25 and 55 vol.% of binder (ink_25 and ink_55), in respect to the powder, were deposited and thermally treated to obtain Cu_2O- and Cu_2O/CuO-based films for further optical and photoelectrochemical characterizations and hydrogen production studies. The increased film porosity obtained using Ink_55 positively affects the electron transfer from the electrode surface to the electrolyte, thus increasing the photocurrent values. The Cu_2O/CuO system is able to extend the light adsorption close to 900 nm and

shows a higher charge carrier density than the system based on Cu_2O (N_A equal to 6.2 and 2.3 × 10^{27} cm^{-3} for ink_55 Cu_2O/CuO and Cu_2O respectively). For these reasons, the highest photocurrent densities are obtained for the mixed Cu_2O/CuO films. An amount of hydrogen equal to 6 and 7 µmol cm^{-2} (after 2 h of operation) was achieved, at slightly acid pH, for ink_25 and ink_55 respectively. After testing, degradation of copper-based layers was observed due to the absence of a protective coating on the electrode. This work highlights the adequacy of the screen-printing technology to produce layers for a hydrogen photoelectrochemical water-splitting reaction. This technique can be considered as a low-cost, simple, and affordable candidate for the realization of water-splitting electrodes, especially in view of the large-scale development of this hydrogen production technology.

Author Contributions: Conceptualization, A.G., N.S. and A.S. (Alessandra Sanson); methodology, A.G. and N.S.; validation, A.G. and N.S.; investigation, N.S., A.G., A.S. (Alex Sangiorgi); resources, A.G.; data curation, N.S., A.G., A.S. (Alex Sangiorgi); writing—original draft preparation, A.G.; writing—review and editing, A.S. (Alessandra Sanson), N.S., A.S. (Alex Sangiorgi); supervision, A.G. and A.S. (Alessandra Sanson); project administration, A.G. All authors have read and agreed to the published version of the manuscript.

Funding: This research was funded by MINISTRY OF DEFENCE, ITALY in the frame of the project SOS-Water.

Institutional Review Board Statement: Not applicable.

Informed Consent Statement: Not applicable.

Data Availability Statement: Not applicable.

Conflicts of Interest: The authors declare no conflict of interest.

References

1. Samsudin, M.F.R.; Sufian, S.; Mohamed, N.M.; Bashiri, R.; Wolfe, F.; Ramli, R.M. Enhancement of Hydrogen Production over Screen-Printed TiO_2/$BiVO_4$ Thin Film in the Photoelectrochemical Cells. *Mater. Lett.* **2018**, *211*, 13–16. [CrossRef]
2. Saraswat, S.K.; Rodene, D.D.; Gupta, R.B. Recent Advancements in Semiconductor Materials for Photoelectrochemical Water Splitting for Hydrogen Production Using Visible Light. *Renew. Sustain. Energy Rev.* **2018**, *89*, 228–248. [CrossRef]
3. Sangiorgi, N.; Tuci, G.; Sanson, A.; Peruzzini, M.; Giambastiani, G. Metal-Free Carbon-Based Materials for Electrocatalytic and Photo-Electrocatalytic CO_2 Reduction. *Rend. Fis. Acc. Lincei* **2019**, *30*, 497–513. [CrossRef]
4. Günnemann, C.; Curti, M.; Eckert, J.G.; Schneider, J.; Bahnemann, D.W. Tailoring the Photoelectrochemical Activity of TiO_2 Electrodes by Multilayer Screen-Printing. *ChemCatChem* **2019**, *11*, 6439–6450. [CrossRef]
5. Marlinda, A.R.; Yusoff, N.; Pandikumar, A.; Huang, N.M.; Akbarzadeh, O.; Sagadevan, S.; Wahab, Y.A.; Johan, M.R. Tailoring Morphological Characteristics of Zinc Oxide Using a One-Step Hydrothermal Method for Photoelectrochemical Water Splitting Application. *Int. J. Hydrogen Energy* **2019**, *44*, 17535–17543. [CrossRef]
6. Masudy-Panah, S.; Kong Eugene, Y.-J.; Dasineh Khiavi, N.; Katal, R.; Gong, X. Aluminum-Incorporated p-CuO/n-ZnO Photocathode Coated with Nanocrystal-Engineered TiO_2 Protective Layer for Photoelectrochemical Water Splitting and Hydrogen Generation. *J. Mater. Chem. A* **2018**, *6*, 11951–11965. [CrossRef]
7. Paracchino, A.; Laporte, V.; Sivula, K.; Grätzel, M.; Thimsen, E. Highly Active Oxide Photocathode for Photoelectrochemical Water Reduction. *Nat. Mater.* **2011**, *10*, 456–461. [CrossRef] [PubMed]
8. Lim, Y.-F.; Chua, C.S.; Lee, C.J.J.; Chi, D. Sol-Gel Deposited Cu_2O and CuO Thin Films for Photocatalytic Water Splitting. *Phys. Chem. Chem. Phys.* **2014**, *16*, 25928–25934. [CrossRef] [PubMed]
9. Hinojosa-Reyes, M.; Camposeco-Solís, R.; Zanella, R.; Rodríguez González, V. Hydrogen Production by Tailoring the Brookite and Cu_2O Ratio of Sol-Gel Cu-TiO_2 Photocatalysts. *Chemosphere* **2017**, *184*, 992–1002. [CrossRef] [PubMed]
10. Dubale, A.A.; Pan, C.-J.; Tamirat, A.G.; Chen, H.-M.; Su, W.-N.; Chen, C.-H.; Rick, J.; Ayele, D.W.; Aragaw, B.A.; Lee, J.-F.; et al. Heterostructured Cu_2O/CuO Decorated with Nickel as a Highly Efficient Photocathode for Photoelectrochemical Water Reduction. *J. Mater. Chem. A* **2015**, *3*, 12482–12499. [CrossRef]
11. Waldner, G.; Krýsa, J. Photocurrents and Degradation Rates on Particulate TiO_2 Layers: Effect of Layer Thickness, Concentration of Oxidizable Substance and Illumination Direction. *Electrochim. Acta* **2005**, *50*, 4498–4504. [CrossRef]
12. Jang, Y.J.; Lee, J.S. Photoelectrochemical Water Splitting with P-Type Metal Oxide Semiconductor Photocathodes. *ChemSusChem* **2019**, *12*, 1835–1845. [CrossRef]

13. Chiang, C.-Y.; Aroh, K.; Franson, N.; Satsangi, V.R.; Dass, S.; Ehrman, S. Copper Oxide Nanoparticle Made by Flame Spray Pyrolysis for Photoelectrochemical Water Splitting—Part II. Photoelectrochemical Study. *Int. J. Hydrogen Energy* **2011**, *36*, 15519–15526. [CrossRef]
14. Chang, Y.; Braun, A.; Deangelis, A.; Kaneshiro, J.; Gaillard, N. Effect of Thermal Treatment on the Crystallographic, Surface Energetics, and Photoelectrochemical Properties of Reactively Cosputtered Copper Tungstate for Water Splitting. *J. Phys. Chem. C* **2011**, *115*, 25490–25495. [CrossRef]
15. Thongthep, P.; Moonmangmee, S.; Ponchio, C. Solar/Photoelectrocatalytic Cell Development for H_2 Production and Simultaneous Organic Dye Degradation. *Mater. Sci. Semicond. Process.* **2021**, *124*, 105597. [CrossRef]
16. Dharmadasa, I.M.; Haigh, J. Strengths and Advantages of Electrodeposition as a Semiconductor Growth Technique for Applications in Macroelectronic Devices. *J. Electrochem. Soc.* **2005**, *153*, 47. [CrossRef]
17. Gondolini, A.; Mercadelli, E.; Sangiorgi, A.; Sanson, A. Integration of Ni-GDC Layer on a NiCrAl Metal Foam for SOFC Application. *J. Eur. Ceram. Soc.* **2017**, *37*, 1023–1030. [CrossRef]
18. Gondolini, A.; Mercadelli, E.; Constantin, G.; Dessemond, L.; Yurkiv, V.; Costa, R.; Sanson, A. On the Manufacturing of Low Temperature Activated $Sr_{0.9}La_{0.1}TiO_{3-\delta}$-$Ce_{1-X}Gd_xO_{2-\delta}$ Anodes for Solid Oxide Fuel Cell. *J. Eur. Ceram. Soc.* **2018**, *38*, 153–161. [CrossRef]
19. Naponiello, G.; Venditti, I.; Zardetto, V.; Saccone, D.; Di Carlo, A.; Fratoddi, I.; Barolo, C.; Dini, D. Photoelectrochemical Characterization of Squaraine-Sensitized Nickel Oxide Cathodes Deposited via Screen-Printing for p-Type Dye-Sensitized Solar Cells. *Appl. Surf. Sci.* **2015**, *356*, 911–920. [CrossRef]
20. Obata, K.; van de Krol, R.; Schwarze, M.; Schomäcker, R.; Abdi, F.F. In Situ Observation of PH Change during Water Splitting in Neutral PH Conditions: Impact of Natural Convection Driven by Buoyancy Effects. *Energy Environ. Sci.* **2020**, *13*, 5104–5116. [CrossRef]
21. Sangiorgi, N.; Aversa, L.; Tatti, R.; Verucchi, R.; Sanson, A. Spectrophotometric Method for Optical Band Gap and Electronic Transitions Determination of Semiconductor Materials. *Opt. Mater.* **2017**, *64*, 18–25. [CrossRef]
22. Murali, D.S.; Kumar, S.; Choudhary, R.J.; Wadikar, A.D.; Jain, M.K.; Subrahmanyam, A. Synthesis of Cu_2O from CuO Thin Films: Optical and Electrical Properties. *AIP Adv.* **2015**, *5*, 047143. [CrossRef]
23. Yang, Y.; Xu, D.; Wu, Q.; Diao, P. Cu_2O/CuO Bilayered Composite as a High-Efficiency Photocathode for Photoelectrochemical Hydrogen Evolution Reaction. *Sci. Rep.* **2016**, *6*, 35158. [CrossRef] [PubMed]
24. Gondolini, A.; Mercadelli, E.; Zin, V.; Barison, S.; Sanson, A. Easy Preparation Method of Stable Copper-Based Nanoparticle Suspensions in Lubricant Engine Oil. *Lubr. Sci.* **2020**, *32*, 205–217. [CrossRef]
25. Moreno, R. Better Ceramics through Colloid Chemistry. *J. Eur. Ceram. Soc.* **2020**, *40*, 559–587. [CrossRef]
26. Gondolini, A.; Fasolini, A.; Mercadelli, E.; Basile, F.; Sanson, A. Freeze Cast Porous Membrane Catalyst for Hydrogen Production via Oxy-Reforming. *Fuel Process. Technol.* **2021**, *213*, 106658. [CrossRef]
27. Sanson, A.; Mercadelli, E.; Roncari, E.; Licheri, R.; Orrù, R.; Cao, G.; Merlone-Borla, E.; Marzorati, D.; Bonavita, A.; Micali, G.; et al. Influence of Processing Parameters on the Electrical Response of Screen Printed $SrFe_{0.6}Ti_{0.4}O_{3-\delta}$ Thick Films. *Ceram. Int.* **2010**, *36*, 521–527. [CrossRef]
28. Sanson, A.; Gardini, D.; Montanari, G.; Galassi, C.; Roncari, E. Key Role of Milling in the Optimization of TiO_2 Nanoinks. *J. Mater. Res.* **2006**, *21*, 1561–1569. [CrossRef]
29. Lanzini, A.; Guerra, C.; Leone, P.; Santarelli, M.; Smeacetto, F.; Fiorilli, S.; Gondolini, A.; Mercadelli, E.; Sanson, A.; Brandon, N.P. Influence of the Microstructure on the Catalytic Properties of SOFC Anodes under Dry Reforming of Methane. *Mater. Lett.* **2016**, *164*, 312–315. [CrossRef]
30. Kim, J.Y.; Rodriguez, J.A.; Hanson, J.C.; Frenkel, A.I.; Lee, P.L. Reduction of CuO and Cu_2O with H_2: H Embedding and Kinetic Effects in the Formation of Suboxides. *J. Am. Chem. Soc.* **2003**, *125*, 10684–10692. [CrossRef] [PubMed]
31. Masudy-Panah, S.; Siavash Moakhar, R.; Chua, C.S.; Tan, H.R.; Wong, T.I.; Chi, D.; Dalapati, G.K. Nanocrystal Engineering of Sputter-Grown CuO Photocathode for Visible-Light-Driven Electrochemical Water Splitting. *ACS Appl. Mater. Interfaces* **2016**, *8*, 1206–1213. [CrossRef]
32. Aktar, A.; Ahmmed, S.; Hossain, J.; Md. Ismail, A.B. Solution-Processed Synthesis of Copper Oxide (CuxO) Thin Films for Efficient Photocatalytic Solar Water Splitting. *ACS Omega* **2020**, *5*, 25125–25134. [CrossRef] [PubMed]
33. Nian, J.-N.; Hu, C.-C.; Teng, H. Electrodeposited P-Type Cu_2O for H_2 Evolution from Photoelectrolysis of Water under Visible Light Illumination. *Int. J. Hydrogen Energy* **2008**, *33*, 2897–2903. [CrossRef]
34. Bagal, I.V.; Chodankar, N.R.; Hassan, M.A.; Waseem, A.; Johar, M.A.; Kim, D.-H.; Ryu, S.-W. Cu_2O as an Emerging Photocathode for Solar Water Splitting—A Status Review. *Int. J. Hydrogen Energy* **2019**, *44*, 21351–21378. [CrossRef]
35. Toe, C.Y.; Scott, J.; Amal, R.; Ng, Y.H. Recent Advances in Suppressing the Photocorrosion of Cuprous Oxide for Photocatalytic and Photoelectrochemical Energy Conversion. *J. Photochem. Photobiol. C Photochem. Rev.* **2019**, *40*, 191–211. [CrossRef]
36. Toe, C.Y.; Zheng, Z.; Wu, H.; Scott, J.; Amal, R.; Ng, Y.H. Photocorrosion of Cuprous Oxide in Hydrogen Production: Rationalising Self-Oxidation or Self-Reduction. *Angew. Chem. Int. Ed.* **2018**, *57*, 13613–13617. [CrossRef]
37. Enzweiler, H.; Yassue-Cordeiro, P.H.; Schwaab, M.; Barbosa-Coutinho, E.; Olsen Scaliante, M.H.N.; Fernandes, N.R.C. Catalyst Concentration, Ethanol Content and Initial PH Effects on Hydrogen Production by Photocatalytic Water Splitting. *J. Photochem. Photobiol. A Chem.* **2020**, *388*, 112051. [CrossRef]

38. Peng, R.; Baltrusaitis, J.; Wu, C.M.; Koodali, R.T. Pd–Ti-MCM-48 Cubic Mesoporous Materials for Solar Simulated Hydrogen Evolution. *Int. J. Hydrogen Energy* **2015**, *40*, 905–918. [CrossRef]
39. Li, C.; He, J.; Xiao, Y.; Li, Y.; Delaunay, J.-J. Earth-Abundant Cu-Based Metal Oxide Photocathodes for Photoelectrochemical Water Splitting. *Energy Environ. Sci.* **2020**, *13*, 3269–3306. [CrossRef]